Optics Letters

Effect of the AlN strain compensation layer on InGaN quantum well red-light-emitting diodes beyond epitaxy

Zhiyuan Liu, Mingtao Nong, Yi Lu, Haicheng Cao, Saravanan Yuvaraja, Na Xiao, Zahrah Alnakhli, Raul Ricardo Aguileta Vázquez, and Xiaohang Li*

King Abdullah University of Science and Technology (KAUST), Advanced Semiconductor Laboratory, Thuwal 23955-6900, Saudi Arabia
**Corresponding author: xiaohang.li@kaust.edu.sa*

Received 28 September 2022; revised 20 October 2022; accepted 21 October 2022; posted 26 October 2022; published 28 November 2022

An atomically thick AlN layer is typically used as the strain compensation layer (SCL) for InGaN-based-red light-emitting diodes (LEDs). However, its impacts beyond strain control have not been reported, despite its drastically different electronic properties. In this Letter, we describe the fabrication and characterization of InGaN-based red LEDs with a wavelength of 628 nm. A 1-nm AlN layer was inserted between the InGaN quantum well (QW) and the GaN quantum barrier (QB) as the SCL. The output power of the fabricated red LED is greater than 1 mW at 100 mA current, and its peak on-wafer wall plug efficiency (WPE) is approximately 0.3%. Based on the fabricated device, we then used numerical simulation to systematically study the effect of the AlN SCL on the LED emission wavelength and operating voltage. The results show that the AlN SCL enhances the quantum confinement and modulates the polarization charges, modifying the device band bending and the subband energy level in the InGaN QW. Thus, the insertion of the SCL considerably affects the emission wavelength, and the effect on the emission wavelength varies with the SCL thickness and the Ga content introduced into the SCL. In addition, the AlN SCL in this work reduces the LED operating voltage by modulating the polarization electric field and energy band, facilitating carrier transport. This implies that heterojunction polarization and band engineering is an approach that can be extended to optimize the LED operating voltage. We believe our study better identifies the role of the AlN SCL in InGaN-based red LEDs, promoting their development and commercialization.

https://doi.org/10.1364/OL.476727

InGaN-based red-light-emitting diodes (LEDs) have attracted increasing interest for numerous applications, such as displays, white light sources, and visible light communication [1,2]. Compared with the performance of commercial InGaN-based blue and green LEDs, that of InGaN-based red LEDs is still poor. The high-In-content (>30%) quantum well (QW) of the LED results in a serious lattice mismatch with the GaN template, leading to degraded crystal quality with high-density defects and suppressed internal quantum efficiency [3]. Moreover, the large polarization difference between the InGaN QW and the GaN quantum barrier (QB) contributes to the quantum-confined Stark effect (QCSE). This separates the electron-hole wave functions and leads to a substantial wavelength shift with increasing injection current [4]. Besides, InGaN-based red LEDs still require a large operating voltage, even higher than that in InGaN-based green LEDs at the same current density [5]. This further decreases the device wall plug efficiency (WPE) and hinders its application and commercialization. Recently, considerable progress has been made in regard to the aforementioned issues. To decrease the QW/template lattice mismatch and improve the In-incorporation capability, InGaNOS pseudo-substrates, lattice-matched or relaxed InGaN templates, porous GaN templates, and a low-In-content InGaN/GaN superlattice (SL) have been used [6–11]. Besides, a low forward voltage InGaN-based red LED was demonstrated on the Ga_2O_3 substrate. The V-pits generated from the InGaN SL region can promote hole injection, therefore achieving a reduced operating voltage [12].

Since Al(Ga)N has a smaller lattice constant than GaN, a thin Al(Ga)N layer can be inserted between the QW and the QB as an interlayer to compensate for the compressive strain during QW growth. With the help of the strain compensation layer (SCL), a higher-In-content QW can be achieved with improved material quality [13–15]. Besides, Al(Ga)N capping on the InGaN was demonstrated to prevent indium desorption and composition fluctuations in the QW during high-temperature GaN QB growth [16]. However, reports studying the effect of an AlN SCL beyond epitaxy in InGaN-based red LEDs are rare. The ultrawide bandgap of the AlN layer provides a considerably higher barrier than that obtained using GaN. It also has a considerable polarization difference with the InGaN QW [17]. Therefore, the insertion of the SCL may strongly influence the electrical and optical performance of LEDs, such as the emission wavelength and operating voltage. Therefore, in this study, we fabricated and characterized a 628-nm InGaN-based red LED. Taking the experimental device as a reference, we then conducted a theoretical study concerning the Al(Ga)N SCL.

An InGaN-based red LED wafer was grown via metalorganic chemical vapor deposition (MOCVD) on a patterned c-plane sapphire substrate. The epitaxy structure primarily included

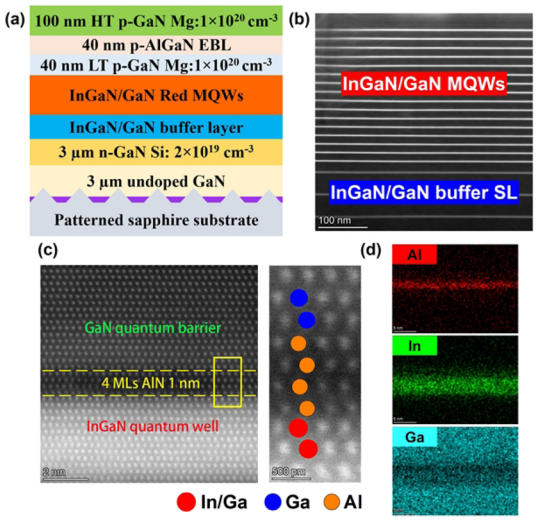

Fig. 1. (a) Schematic of a grown InGaN-based red LED wafer. (b) Cross-sectional TEM image of the InGaN/GaN buffer superlattice (SL) and red multi-quantum wells (MQWs). (c) TEM image of the quantum well (QW) structure with a 1-nm AlN strain compensation layer (SCL). (d) EDX element distribution in the GaN/InGaN/AlN/GaN QW structure.

a sputter AlN, an undoped GaN template, an n-GaN electron injection layer, 3 pairs of InGaN (4 nm)/GaN(40 nm) SLs (PL emission at around 420 nm), 16 pairs of InGaN (3.6 nm)/GaN (12 nm) red multi-quantum wells (MQWs), a p-AlGaN electron blocking layer (EBL), and a p-GaN hole injection layer. Figure 1(a) shows more details concerning the layer thickness and doping; and Fig. 1(b) presents cross-sectional transmission electron microscopy (TEM) images of the InGaN/GaN buffer SL and red MQWs. Significantly, a 4-monolayer (~1-nm) AlN layer was inserted between the InGaN QW and the GaN QB, serving as the SCL. The corresponding TEM image and element distribution measured by energy-dispersive x-ray (EDX) are shown in Figs. 1(c) and 1(d), respectively. The device fabrication process and measurement setup are shown in section S1 of Supplement 1.

Figure 2(a) shows the I–V curve of the fabricated red LED. The operating voltage at 10 A/cm^2 is approximately 3.25 V, which may be limited by the poor current spreading resulting from the large mesa size. The reverse leakage current is around

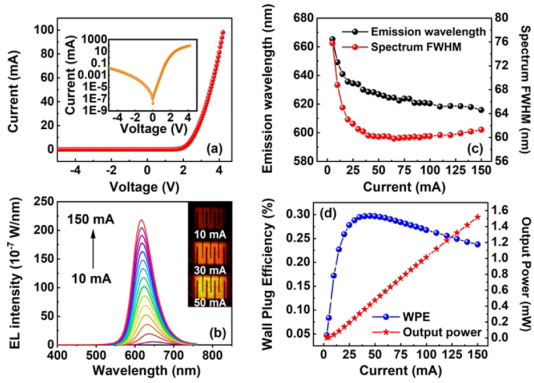

Fig. 2. LED characterization: (a) I–V curve, (b) EL spectrum and an optical image, (c) emission wavelength and FWHM under different currents, and (d) output power and WPE as functions of the injected current.

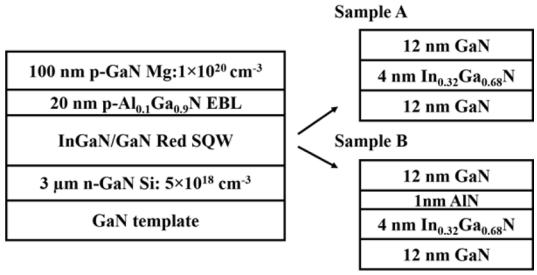

Fig. 3. Simplified LED models with and without an inserted AlN SCL.

10^{-5} A at a reverse voltage of 5 V. The defects from the bulk material and the sidewall damage induced by plasma etching contribute to the leakage path, which can be suppressed by improving the material quality and effective sidewall treatment [18]. Figure 2(b) shows the electroluminescence (EL) spectrum for injection currents from 10 to 150 mA. As seen, no parasitic blue emission is observed, indicating a suppressed phase separation and In fluctuation effect during high-In-content QW growth [19]. The inset optical image shows red and orange–red emissions at different currents. The emission wavelength at 45 mA (at a current density of 14 A/cm^2) is approximately 628 nm. Figure 2(c) shows the change in wavelength and full width at half-maximum (FWHM) with increasing current. The emission wavelength shifts from 665 to 616 nm at 5–150 mA. This huge wavelength shift occurs because of the band-filling effect and QCSE [20]. Moreover, at a low current, the FWHM decreases with increasing injection current from 75.8 to 59.8 nm due to potential fluctuations [21]; at a higher current, the FWHM increases and reaches 61.3 nm at 150 mA, which is related to heat generation [22]. Figure 2(d) shows the output power and WPE under various currents. The output power presents a near-linear increase and is higher than 1 mW at a current of 100 mA. In addition, a 0.3% peak WPE is observed at 45 mA. At higher injection currents, the LED shows a decrease in efficiency. Reports on theoretical models and simulation studies of InGaN-based red LEDs are rare. One reason is the large polarization difference between the high-In-content QW and the GaN QB, which results in convergence problems and poor simulation accuracy for complex LED structures. Therefore, simplifying the structure is the most straightforward method to eliminate this issue. Based on our fabricated device, we built a simplified InGaN-based red LED model (Fig. 3). The device size was the same as that of the aforementioned experimental device to ensure they had a similar current density at the same current. The LED structure contained a GaN template, a 3-μm n-GaN layer with 5×10^{18} cm^{-3} Si doping, a 4-nm/12-nm $In_{0.32}Ga_{0.68}N$/GaN red single QW (SQW), a 20-nm p-$Al_{0.1}Ga_{0.9}N$ EBL, and a 100-nm p-GaN hole injection layer. The p-type layers had 5×10^{18} and 1×10^{20} cm^{-3} Mg doping, respectively. Two QW structures, those without (sample A) and with (sample B) the AlN SCL, were investigated. In this study, we employed the APSYS software from Crosslight for the numerical study [23]. The Auger recombination coefficient was set to 1.0×10^{-30} cm^{-3}, and the Shockley–Read–Hall recombination lifetime was 50 ns [24]. As a result of defect screening, the polarization factor used in this study was 0.6 [25]. The device worked under a temperature of 300 K with an estimated background loss of 2000 m^{-1} [25]. Other parameters were set to their default values in the APSYS software, and we list some of them in section S2 of Supplement 1.

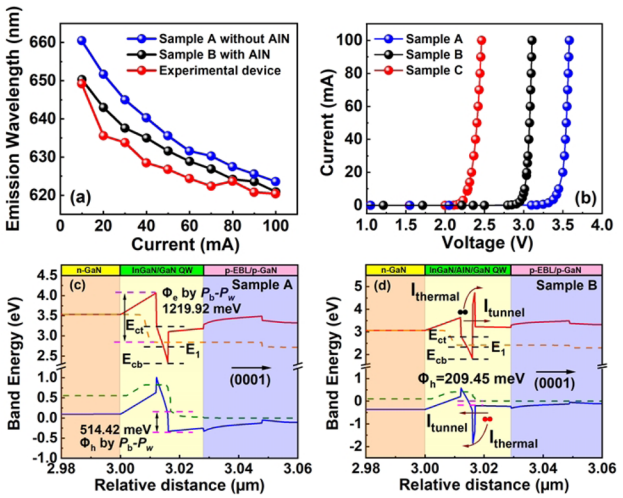

Fig. 4. (a) LED emission wavelengths under different currents and (b) I–V characteristics of the simulated devices. Band diagrams of the simulated InGaN-based red LEDs at 45 mA for (c) sample A and (d) sample B.

Figure 4(a) shows the emission wavelengths of samples A and B under different currents. Sample B shows a similar wavelength and wavelength shift from 10 to 100 mA compared with those of the experimental device. Compared with that of sample B, sample A without the SCL exhibits a longer wavelength at the same current (~633 and 637 nm, respectively, at 45 mA). To explain this, we investigated the band diagrams of samples A and B shown in Figs. 4(c) and 4(d), respectively. Because of the QCSE, the band of the InGaN QW suffers from severe tilting. The bottom and top energies of the QW conduction band are labeled E_{cb} and E_{ct}, respectively. The first conduction subband level resulting from the quantum confinement is labeled E_1. $E_{ct} - E_{cb}$ represents the degree of band tilting; $E_1 - E_{cb}$ and $E_{ct} - E_1$ reflect the transition energies of the recombined electrons.

Table 1 lists the $E_{ct} - E_{cb}$, $E_1 - E_{cb}$, and $E_{ct} - E_1$ values of samples A and B at 45 mA. The $E_{ct} - E_{cb}$ value of sample B (981.34 meV) is greater than that of sample A (906.86 meV) due to the huge polarization difference between InGaN and AlN. Therefore, compared with that of sample A, sample B suffers from a stronger band tilting. However, the AlN layer provides another high barrier for InGaN, which is contributed by its ultra-wide bandgap (around 6.1 eV) and results in a deep QW. Based on quantum mechanics, the first subband level E_1 will therefore be raised. Compared with sample A, sample B increases the value of $E_1 - E_{cb}$ (from 398.44 to 485.24 meV) and reduces the value of $E_{ct} - E_1$ (from 508.42 to 496.10 meV). Therefore, electrons in sample B have a higher transition energy and a shorter emission wavelength than those in sample A.

Figure 4(b) shows the I–V curves of samples A, B, and C. Sample C has the same structure as sample A, but the polarization charge was not considered in the calculation. The knee voltage of sample B is similar to that of the experimental device (~3 V), suggesting a high-accuracy setting for the polarization charge and the QW structure in our simulation model. The results reveal that sample C has a much lower operating voltage than those of samples A or B (~2.4 V at 45 mA). The band diagram of sample A [Fig. 4(c)] shows that the conduction bands in the first and second GaN QBs tilt upward due to the effect of the polarization charges. This leads to extra electron effective barriers Φ_e (~1219.92 meV); therefore, high energy and voltage are required to flow through the GaN layers. Similarly, the valence band is bent toward high energy, leading to a 514.42-meV effective hole barrier Φ_h at the InGaN/GaN interface, indicating poor hole injection. Therefore, we can conclude that the polarization charge negatively affects the operating voltage, thus decreasing the device efficiency. After inserting an AlN layer into sample B, the operating voltage is significantly decreased compared with that of sample A (from 3.53 to 3.07 V at 45 mA). The band diagram of sample B is shown in Fig. 4(d). The inserted thin AlN layer modulates the polarization electric field in the second GaN QB and makes the valence band bend in the opposite way to that of sample A. Therefore, the effective hole barrier at the AlN/GaN interface is diminished from 514.42 to 209.45 meV. Thus, the obstacle is essentially diminished for holes transported in the GaN. As shown in the band diagram, the AlN layer has a large valence band offset with GaN, resulting in a huge barrier for holes. However, the SCL layer is sufficiently thin that holes can pass through the AlN layer via tunneling, not only by thermal excitation. Therefore, the SCL will not limit hole injection into the QW. Similarly, electrons can also pass through the AlN barrier utilizing the tunneling effect. In addition, the conduction band energy decreases along the *c* axis in the second GaN QB, which can help electrons move to the next QW if the LED has an MQW structure. Besides, no obvious IQE change was observed after the AlN insertion, which is discussed in section S3 of Supplement 1.

Table 1. $E_{ct} - E_{cb}$, $E_1 - E_{cb}$, and $E_{ct} - E_1$ of Samples A and B at 45 mA

	$E_{ct} - E_{cb}$ (meV)	$E_1 - E_{cb}$ (meV)	$E_{ct} - E_1$ (meV)
Sample A	906.86	398.44	508.42
Sample B	981.34	485.24	496.10

During the MOCVD process, the AlN SCL was achieved via the Al-source short-time purge after QW growth. The thickness of the grown AlN layer can be difficult to precisely control. Accordingly, we investigated the influence of the thickness of the AlN layer on the emission wavelength and operating voltage of the device. Four samples with two- to six-monolayer (0.5–1.5 nm) SCLs were simulated. In addition, during AlN growth, residual Ga in the MOCVD chamber may form AlGaN with different Ga contents instead of pure AlN. Therefore, we also examined the effect of the Ga content introduced into the SCL.

Figures 5(a)–5(d) show the changes in wavelength and voltage as a function of the thickness and composition of the SCL. The emission wavelength increases with an increase in the AlN layer thickness, especially beyond 1 nm, even though the confinement on the InGaN QW becomes stronger with thicker AlN. It is well known that the intensity of the polarization electric field in a QW increases with an increase in the QB thickness [26]. Therefore, the transition energy decreases because the polarization effect is more dominant than the quantum confinement, leading to more serious band tilting and displacement of the subband level downward. The dominance of the quantum confinement and polarization effect determines the trend in the LED wavelength. Meanwhile, a thicker AlN layer results in a more intense modulation of the polarization electric field and band bending in GaN QBs. As discussed above, this modulation may facilitate carrier transport. Therefore, the operating voltage is reduced with a thicker AlN layer. However, a thicker AlN SCL would suppress the carrier tunneling possibility [27]. The rate of

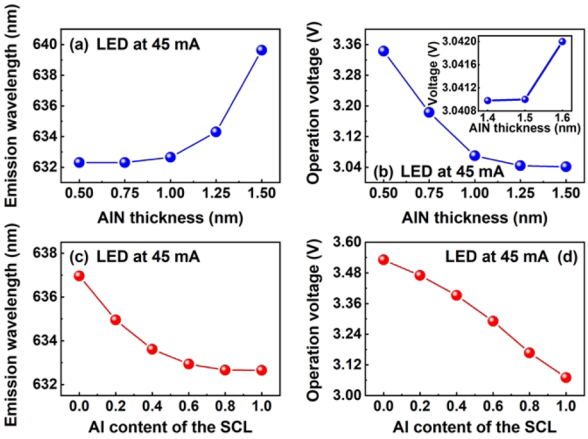

Fig. 5. (a) Emission wavelength and (b) operating voltage at 45 mA for samples with 0.5-nm to 1.5-nm AlN layers. (c) Emission wavelength and (d) operating voltage at 45 mA for 1-nm AlGaN layers with different Al compositions ranging from 0% to 100%.

decrease in the operating voltage gradually reduces with increasing AlN thickness. As shown in the inset figure in Fig. 5(b), the voltage even has a rising trend for the AlN thickness beyond 1.4 nm. Therefore, a thick AlN SCL could be harmful to the device's capabilities, e.g., leading to more heat generation and suppressed device efficiency, although it can compensate for more strain during QW growth.

Similarly, a lower-Al-content SCL results in the quantum confinement being undermined, achieving a lower subband energy level, a smaller transition energy, and a longer wavelength [Fig. 5(c)]. In addition, a lower-Al-content SCL has a smaller polarization difference with InGaN and GaN, contributing to less polarization and band modulation. Accordingly, in Fig. 5(d), we observe an increased operating voltage when the SCL has a low Al content.

In summary, we fabricated and characterized a 628-nm InGaN-based red LED and conducted a series of numerical studies concerning the AlN SCL. The results show that an SCL considerably influences the emission wavelength. Depending on the dominance of the quantum confinement and polarization effect, the emission wavelength varies according to the layer thickness and Ga content introduced into the SCL. In addition, we found that the large polarization electric field inside the LED is the primary reason for the large operating voltage in current InGaN-based red LEDs. Furthermore, the AlN SCL in our study can substantially reduce the operating voltage via polarization and band modulation. Our study indicates that reducing the polarization of the electric field is essential to achieve InGaN-based red LEDs with a low operating voltage; and heterojunction polarization engineering is a promising path for future device optimization. For example, we employed an AlN SCL in this study, a polarization-matched MQW in our previous study, and a staggered InGaN QW in Zhao *et al.*'s work [28,29]. We hope that this paper will increase interest in this topic and aid in the development and commercialization of high-performance InGaN-based red LEDs.

Funding. KAUST Baseline Fund (BAS/1/1664-01-01); KAUST Competitive Research Grants (URF/1/3437-01-01, URF/1/3771-01-01); KAUST Near-Term Grand Challenge Fund (REI/1/4999-01-01); KAUST Impact Acceleration Fund (REI/1/5124-01-01).

Disclosures. The authors declare no conflicts of interest.

Data availability. Data underlying the results presented in this paper are not publicly available at this time but may be obtained from the authors upon reasonable request.

Supplemental document. See Supplement 1 for supporting content.

REFERENCES

1. M. S. Wong, S. Nakamura, and S. P. DenBaars, ECS J. Solid State Sci. Technol. **9**, 015012 (2020).
2. H. S. Wasisto, J. D. Prades, J. Gülink, and A. Waag, Appl. Phys. Rev. **6**, 041315 (2019).
3. R. C. White, H. Li, M. Khoury, C. Lynsky, M. Iza, S. Keller, D. Sotta, S. Nakamura, and S. P. DenBaars, Crystals **11**, 1364 (2021).
4. J. H. Ryou, P. D. Yoder, J. Liu, Z. Lochner, H. Kim, S. Choi, H. J. Kim, and R. D. Dupuis, IEEE J. Sel. Top. Quantum Electron. **15**, 1080 (2009).
5. Z. Zhuang, D. Iida, and K. Ohkawa, Opt. Lett. **46**, 1912 (2021).
6. A. Dussaigne, P. Le Maitre, H. Haas, J. C. Pillet, F. Barbier, A. Grenier, N. Michit, A. Jannaud, R. Templier, D. Vaufrey, and F. Rol, Appl. Phys. Express **14**, 092011 (2021).
7. Z. Bi, T. Lu, J. Colvin, E. Sjogren, N. Vainorius, A. Gustafsson, J. Johansson, R. Timm, F. Lenrick, R. Wallenberg, and B. Monemar, ACS Appl. Mater. Interfaces **12**, 17845 (2020).
8. T. Ozaki, M. Funato, and Y. Kawakami, Appl. Phys. Express **12**, 011007 (2019).
9. S. S. Pasayat, C. Gupta, M. S. Wong, R. Ley, M. J. Gordon, S. P. DenBaars, S. Nakamura, S. Keller, and U. K. Mishra, Appl. Phys. Express **14**, 011004 (2020).
10. P. Li, H. Li, M. S. Wong, P. Chan, Y. Yang, H. Zhang, M. Iza, J. S. Speck, S. Nakamura, and S. P. Denbaars, Crystals **12**, 541 (2022).
11. S. Zhou, X. Liu, H. Yan, Y. Gao, H. Xu, J. Zhao, Z. Quan, C. Gui, and S. Liu, Sci. Rep. **8**, 11053 (2018).
12. D. Iida, Z. Zhuang, P. Kirilenko, M. Velazquez-Rizo, and K. Ohkawa, Appl. Phys. Express **13**, 031001 (2020).
13. D. Iida, S. Lu, S. Hirahara, K. Niwa, S. Kamiyama, and K. Ohkawa, J. Cryst. Growth **448**, 105 (2016).
14. C. M. Tsai, C. S. Chang, Z. Xu, W. P. Huang, W. C. Lai, and J. S. Bow, OSA Continuum **2**, 1207 (2019).
15. J. I. Hwang, R. Hashimoto, S. Saito, and S. Nunoue, Appl. Phys. Express **7**, 071003 (2014).
16. A. I. Alhassan, R. M. Farrell, B. Saifaddin, A. Mughal, F. Wu, S. P. DenBaars, S. Nakamura, and J. S. Speck, Opt. Express **24**, 17868 (2016).
17. G. Tao, X. Zhao, and S. Zhou, Opt. Lett. **46**, 4593 (2021).
18. R. T. Ley, J. M. Smith, M. S. Wong, T. Margalith, S. Nakamura, S. P. DenBaars, and M. J. Gordon, Appl. Phys. Lett. **116**, 251104 (2020).
19. T. Mukai, M. Yamada, and S. Nakamura, Jpn. J. Appl. Phys. **38**, 3976 (1999).
20. S. Yamamoto, Y. Zhao, C. C. Pan, R. B. Chung, K. Fujito, J. Sonoda, S. P. DenBaars, and S. Nakamura, Appl. Phys. Express **3**, 122102 (2010).
21. F. Akyol, D. N. Nath, E. Gür, P. S. Park, and S. Rajan, Jpn. J. Appl. Phys. **50**, 052101 (2011).
22. V. Rienzi, J. Smith, N. Lim, H. M. Chang, P. Chan, M. S. Wong, M. J. Gordon, S, P. DenBaars, and S. Nakamura, Crystals **12**, 1144 (2022).
23. "APSYS," Crosslight Software, Inc., 2020, http://www.crosslight.com.
24. J. Piprek, F. Römer, and B. Witzigmann, Appl. Phys. Lett. **106**, 101101 (2015).
25. Z. Liu, Y. Lu, Y. Wang, R. Lin, C. Xiong, and X. Li, IEEE Photonics J. **14**, 8210208 (2021).
26. Z. H. Zhang, W. Liu, Z. Ju, S. Tiam Tan, Y. Ji, Z. Kyaw, X. Zhang, L. Wang, X. Wei Sun, and H. Volkan Demir, Appl. Phys. Lett. **104**, 243501 (2014).
27. C. Chu, K. Tian, J. Che, H. Shao, J. Kou, Y. Zhang, Y. Li, M. Wang, Y. Zhu, and Z. H. Zhang, Opt. Express **27**, A620 (2019).
28. H. H. Yao, Y. Lu, K. H. Li, F. Al-Qatari, C. H. Liao, and X. Li, Proc. SPIE **10940**, 73 (2019).
29. X. Zhao, B. Tang, L. Gong, J. Bai, J. Ping, and S. Zhou, Appl. Phys. Lett. **118**, 182102 (2021).